Measuring accurately liquid and tissue surface tension with a compression plate tensiometer

Abbas Mgharbel,[1] Hélène Delanoë-Ayari,[1] and Jean-Paul Rieu[1]

[1]Université de Lyon, Université de Lyon I, Laboratoire de Physique de la Matière Condensée et des Nanostructures, CNRS, UMR 5586, 43 Boulevard du 11 Nov. 1918, 69622 Villeurbanne Cedex, France

(Received 30 January 2009; accepted 20 March 2009; published online 28 April 2009)

Apparent tissue surface tension allows the quantification of cell-cell cohesion and was reported to be a powerful indicator for the cellular rearrangements that take place during embryonic development or for cancer progression. The measurement is realized with a parallel compression plate tensiometer using the capillary laws. Although it was introduced more than a decade ago, it is based on various geometrical or physical approximations. Surprisingly, these approximations have never been tested. Using a novel tensiometer, we compare the two currently used methods to measure tissue surface tension and propose a third one, based on a local polynomial fit (LPF) of the profile of compressed droplets or cell aggregates. We show the importance of measuring the contact angle between the plate and the drop/aggregate to obtain real accurate measurement of surface tension when applying existing methods. We can suspect that many reported values of surface tension are greatly affected because of not handling this parameter properly. We show then the benefit of using the newly introduced LPF method, which is not dependent on this parameter. These findings are confirmed by generating numerically compressed droplet profiles and testing the robustness and the sensitivity to errors of the different methods. [DOI: 10.2976/1.3116822]

CORRESPONDENCE
Jean-Paul Rieu:
rieu@lpmcn.univ-lyon1.fr

It is now well admitted that mechanics plays a fundamental role in tissue organization and genesis (Lecuit and Lenne, 2007). To get to their final position, cells need to move or more exactly to flow as liquids (Cui *et al.*, 2005). But what are the physical characteristics driving or resisting these cells movements? What are their biological origins? To answer these questions, one has to keep in mind that tissues are complex materials which do present visco-elasto-plastic behavior. Tissues submitted to forces (either external forces as the compression force applied in this work or internal forces occurring during morphogenetic movements) behave like plastic materials because cells gradually rearrange and change neighbors (Brodland *et al.*, 2006). However depending on time scales, this complexity can often be simplified. At short time scales (0–10 min), tissues respond mostly as visco-elastic solids (Forgacs *et al.*, 1998; Phillips and Steinberg, 1978). At long time scales (hours or days depending on the cell type), certain embryonic tissues mimic the behavior of highly viscous liquid droplets (Beysens *et al.*, 2000). In the absence of external forces, irregular tissue fragments or aggregates of reaggregated cells round up into spherical shapes and fuse when they are brought into mutual contact (Gordon *et al.*, 1972). The engulfment of one tissue type by another via spreading, and the sorting of cell types in heterotypic mixtures are other examples of liquidlike behaviors (Steinberg, 1962, 1970; Technau and Holstein, 1992). The very same final tissue configuration could be arrived at by an entirely different pathway (i.e., sorting-out or spreading; Steinberg, 1963, 1970). All these processes are similar to the rounding-up, coalescence or demixing of immiscible liquids which are driven by surface tension σ and resisted by viscosity η (Gordon *et al.*, 1972). Interestingly enough, these two quantities are accessible experimentally. In the case of tissues, the apparent surface tension is

measured using a compression plate tensiometer (Foty *et al.*, 1994) while the apparent viscosity follows from the analysis of aggregate shape relaxation kinetics (Gordon *et al.*, 1972; Rieu and Sawada, 2002; Mombach *et al.*, 2005; Jakab *et al.*, 2008a).

Steinberg proposed that cell sorting is driven by surface energy minimization, arising from cellular adhesive interactions [differential adhesion hypothesis, (DAH) (Steinberg, 1963)]. He concluded that mixed populations of sufficiently mobile cells rearrange so that the less cohesive cells envelop the more cohesive ones (Steinberg, 1970). Experimentally, measurements of apparent aggregate surface tensions have shown that a cell aggregate of lower surface tension tends to envelop one of higher surface tension to which it adheres (Foty *et al.*, 1996). The link between surface tension and adhesive molecules expressed by tissues was done using L cell aggregates transfected to express N-, P-, or E-cadherin in varied, measured amounts: a direct, linear correlation was observed between apparent surface tension and cadherin expression level (Foty and Steinberg, 2005; Hegedüs *et al.*, 2006). Other factors, such as cell contractility and rigidity, have been suggested to play a role in cell sorting, but have not yet been explored extensively (Harris, 1975; Brodland, 2002; Krieg *et al.*, 2008).

For biological applications, tissue surface tensiometry is a new technology to explore fundamental issues regarding cell-cell and cell-substratum interaction in (i) morphogenesis, (ii) cancer progression, and (iii) tissue engineering. Foty and Steinberg (2004) and Marga *et al.* (2007) recently reviewed these issues, which we briefly summarize here.

(i) The analysis of surface tension and sorting/envelopment behavior of germ layer progenitor cells in amphibians (Davis *et al.*, 1997) and zebrafish (Schötz *et al.*, 2008) suggests that surface tension is involved in guiding germ layer morphogenesis during gastrulation. Downregulation of E-cadherin levels in the later study leads to a decrease in the measured surface tension and a corresponding reversal of germ layer positioning in cell sorting experiments.

(ii) It is generally assumed that the invasiveness of cancer cells largely depends on a loss of cell cohesion. Cadherins have been linked with transition to malignancy for a variety of tumors. In particular, the expression of E-cadherin often, but not always, inversely correlates with tumor aggressiveness (Foty and Steinberg, 2004). However, for brain tumors, it was shown that dexamethasone mediated decreased invasiveness correlates with increased aggregate surface tension (i.e., cohesivity) but not with N-cadherin expression (Winters *et al.*, 2005). Surface tension represents a global property of a tissue that may depend on other interactions than the only cadherin-cadherin interactions. $\alpha 5\beta 1$ integrin-fibronectin interactions can indeed mediate strong cohesion (Robinson *et al.*, 2003). The interactions of a cell with the surrounding matrix are also, of course, very important to control the invasive properties of tumors (Hegedüs *et al.*, 2006).

(iii) Tissue engineering aims at reproducing morphogenesis in the laboratory, i.e., to fabricate replacement organs for regenerative medicine. It has been shown that the liquid properties of some tissues, in particular the capability to fuse or reaggregate, may be used to self-assemble cellular aggregates into 3D living structures (Jakab *et al.*, 2004; Jakab *et al.*, 2008b; Marga *et al.*, 2007). Surface tension and viscosity are parameters that can be used both experimentally and theoretically to control and predict this self- or reassembly. In addition, surface tension can also strongly influence the ability of tissues to interact with other biomaterials (Ryan *et al.*, 2001).

Although a new method based on centrifugation followed by axisymmetric drop shape analysis has been recently described (Kalantarian *et al.*, 2009) the most widely used quantitative method to measure the apparent tissue surface tension (σ) is by compression plate tensiometry (Foty *et al.*, 1994; Hegedüs *et al.*, 2006). As cell aggregates behave as solid elastic materials at short time scales, it is also possible to follow their viscoelastic response at short time scales with this apparatus (Forgacs *et al.*, 1998). At long time scales, once elastic forces are relaxed, σ is measured assuming that cell aggregates verify the same physical laws of capillarity as liquid droplets.

When a droplet is compressed between two identical plates (i.e., with identical surface properties), it has a rotational symmetry around the z-axis and a reflection symmetry with respect to its equatorial plane, in which it has the two principal radii of curvatures R_1 and R_2 shown in Fig. 1(A). R_3 is the radius of the droplet's circular area of contact with the compression plates. The compression force F applied to the upper (or lower) plate is balanced by two capillary forces each proportional to σ. The first one is due to the excess pressure inside the drop due to curvature given by the Laplace formula $\Delta p = \sigma(1/R_1 + 1/R_2)$. When the radii of curvature are positive as it is generally the case with cellular aggregates, this first term is always positive (i.e., repulsion between the two plates). The second term is proportional to the drop perimeter and is always negative (i.e., attraction between the two plates). For an arbitrary horizontal plane, at mechanical equilibrium, the equilibrium condition when evaluated along the vertical axis implies $F = \Delta p A - \sigma P \sin\phi$. Here A and P represent the cross-sectional area and the perimeter of the liquid drop in this plane, respectively, and ϕ is the angle between the horizontal and the tangent to the profile of liquid drop at the plane. For the horizontal boundary plane located just underneath the upper plate, $A = \pi R_3^2$, $P = 2\pi R_3$, and $\phi = \theta$, the complementary contact angle [Fig. 1(A)]. Thus, by using the Laplace formula for Δp, one obtains

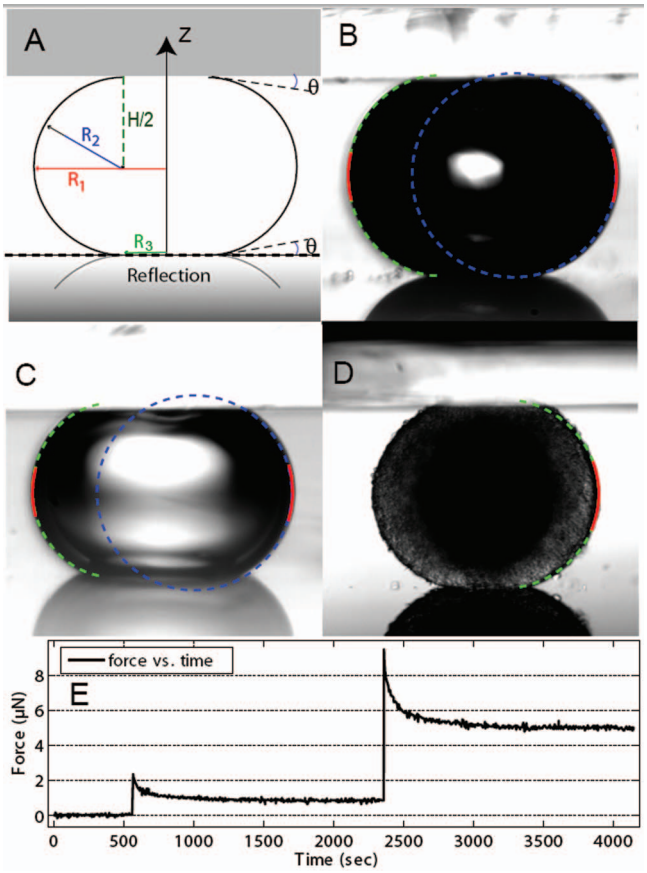

Figure 1. (A) Diagram of a liquid droplet compressed between two parallel plates with a contact angle θ. At equilibrium, R_1 and R_2 are the two primary radii of curvature, at the droplet's equator and in a plane through its axis of symmetry, respectively. R_3 is the radius of the droplet's circular area of contact with either compression plate. H is the distance between upper and lower compression plates. The reflected profile on the bottom plate visible in (B)–(D) is also represented on this diagram. (B)–(D) Snapshots of compressed droplets: (B) air bubble ($R_1=282$ μm) in culture medium, (C) water droplet ($R_1=207$ μm) in mineral oil, and (D) mouse embryonic cell aggregate ($R_1=297$ μm) in culture medium. Red curves correspond to the calculated profile with a second order polynomial fit (LPF method), dotted lines correspond to the calculated profiles with the exact Laplace profile method (ELP, green) and the circular arc approximation (blue). The latter is not represented in order to appreciate the embryonic aggregate roughness in (D). (E) Force signal as measured by our cantilever and an eddy current position sensor: the peaks of force just after a compression are followed by a force relaxation period of about 10 min. We measured the force and shape parameters for the surface tension evaluation at least 30 min after the compression step.

$$F=\left(\pi R_3^2\left(\frac{1}{R_1}+\frac{1}{R_2}\right)-2\pi R_3\sin\theta\right)\sigma=L_P\sigma, \tag{1}$$

where L_P is therefore just a geometrical parameter depending on R_1, R_2, R_3, and θ. Similarly, for the median plane of the compressed drop at $H/2$, where H is the compressed drop height, one has $A=\pi R_1^2$, $P=2\pi R_1$, and $\phi=\pi/2$. The force depends on the geometrical parameter L_M:

$$F=\pi R_1\left(\frac{R_1}{R_2}-1\right)\sigma=L_M\sigma. \tag{2}$$

These two equations are equivalent as the force in each droplet horizontal plane is of course conserved along the vertical axis. While R_1 and F can be accurately measured, the determination of σ from either one of these two equations requires the measured values for R_2 and/or θ and R_3 that can only be obtained with large errors. In earlier published studies this problem has been circumvented by making the approximation that the lateral profile of the drop is a portion of circular arc (Foty *et al.*, 1996; Schötz *et al.*, 2008):

$$R_3=R_1-R_2+\sqrt{R_2^2-(H/2)^2}. \tag{3}$$

In order to even simplify the analysis, plates are generally treated to prevent aggregate/plate adhesion and it is assumed that $\theta=0°$, $R_2=H/2$, and $R_3=R_1-R_2$ (Davis *et al.*, 1997).

Norotte *et al.* (2008) have used another method based on the exact solution of the Laplace equation and on the only measurements of H and R_1. They claim their method is weakly sensitive on the angle, as long as $\theta\leqslant 20°$. They also claim that the previously existing method, based on the circular arc approximation (CA method), fails to give consistent results in a certain range of the compressive force or contact angle. But they did not present any quantitative analysis on the geometrical parameter sensibility of the different methods.

Although, the exact Laplace profile (ELP) method in principle uses exact thermodynamics and gives a rigorous estimation of surface tension in the case of liquid droplets, we found that it still requires the use of experimental parameters θ and H that may suffer large experimental errors. Imposing $\theta\approx 0°$ may sometimes be difficult because cell aggregates may adhere to the plates after prolonged compression despite the fact that coating minimizing adhesion is used. In our experience, θ may vary during a compression experiment and H is a difficult parameter to measure optically with high accuracy because of a number of interfering factors such as the large field of focus, the imperfect parallelism between plates, light multi-reflections or optical aberrations. In this study we used the force signal to determine the exact position a which the upper plate contacts the droplet. H is easily obtained from the aggregate height before compression by subtracting the motor vertical displacement done to compress the aggregate from this position and by adding the deflection of the cantilever. For this method the resolution depends on the force signal sensitivity (0.1 μN for our study) and the Z-motor minimal step (0.04 μm here).

The motivation for the present work is to establish a more direct and robust method to measure the absolute values of apparent tissue surface tensions accurately and reliably independent of the contact angle. It is based on a direct measure-

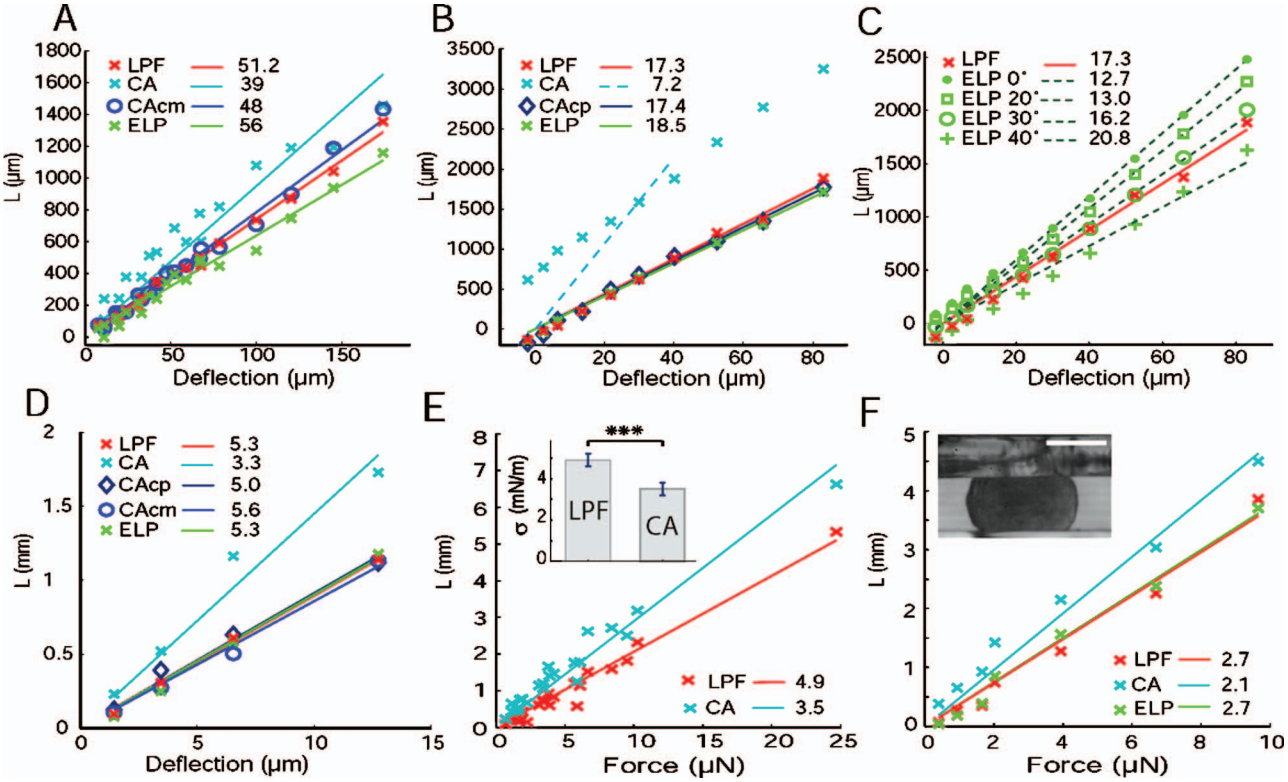

Figure 2. Plots of the geometrical parameters L_P, L_M and L_E as a function of cantilever deflection δ (A–D) or force F (E,F). Surface tension values (displayed in the legend in mN/m) are obtained by taking the slope of the obtained linear fits, with L_P, L_M, and L_E obtained as defined in Eqs. (1), (3), and (5), and $\delta = F/k$ (with $k \sim 0.36$ N/m for all experiments). Air bubble in CO_2 independent culture medium at 37 °C (A), water droplet in mineral oil at room temperature (B,C), F9 embryonic cell aggregate in CO_2 independent culture medium at 37 °C (D,E), and chicken embryonic neural retina aggregate in CO_2 independent culture medium at 37 °C (F). In the inset of (E), we show that the difference between the mean measured values with each method is statistically significant. In the inset of (F), we show a snapshot of compressed neural aggregate (bar, 200 μm). Abbreviations of the different methods tested are as follows: ELP, exact Laplace profile; LPF, local polynomial fit; CA: circular arc; CAcm, circular arc with force calculated at median plane; CAcp, circular arc with force calculated on plates.

ment of R_1 and R_2 using a local polynomial fit (LPF) at equatorial plane and Eq. (2). In addition, we compare the three existing methods (CA, ELP, and LPF methods) and evaluate their respective sensitivity to experimental errors. For that purpose we have performed compression experiments on water drops in mineral oil (W-O), air bubbles in culture medium (A-M), and embryonic cell aggregates in culture medium (C-M) with a self-made tissue tensiometer. We have also evaluated the robustness and the sensitivity to errors of the three methods by generating numerically compressed droplet profiles.

RESULTS

We first compressed air bubbles in culture medium (CO_2 independent medium, 37 °C). These bubbles are easily nucleated by pouring cold medium on the tensiometer plates already at 37 °C and waiting 2 h for temperature stabilization. The complementary contact angle θ is small when glass is clean and hydrophilic. But because glass surfaces are frequently reused, θ may change from one experiment to the other, or after successive compressions. Only for half of the compressions investigated ($n=20$ compression-steps corresponding to three different bubbles) could we really obtain an angle $\theta \leqslant 5°$ for all four recorded glass/air/medium contact lines [Fig. 1(B)]. The angle was comprised between 10° and 25° otherwise. Figure 2(A) shows the plot of geometrical parameters L_P, L_M, or L_E defined in Eqs. (1), (2), and (5) for each method as a function of the deflection transmitted to the upper plate ($\delta = F/k$ where F is the force). The points in the graph correspond to three different bubbles. This plot displays a linear relationship between δ and L for each method, as expected from capillary laws, and the slope k/σ gives the surface tension σ. However, with ELP and CA methods, points are much dispersed and the surface tension values ($\sigma = 56 \pm 2.6$ and 39 ± 3.1 mN/m, respectively) are significantly different from a direct measurement using the wilhelmy plate pressure sensor of a Langmuir trough (NIMA, England): $\sigma = 51 \pm 2$ mN/m. In contrast, the LPF method provides the correct value, with the lower error: $\sigma = 51.2 \pm 1.2$ mN/m. When it is calculated at the median

plane, the circular arc approximation (CAcm) gives also a reasonable agreement although the value is slightly lower (σ=48±1.4 mN/m).

We followed up our study by compression analysis of water droplet, immerged in mineral oil (Sigma) at room temperature. The complementary contact angle was approximately θ=28±5° for the five investigated droplets, with minimal changes from one compression to the other. The original CA method that ignores such a large angle [i.e., it uses Eqs. (1) and (3) with θ=0°] gives clearly an underestimated surface tension. The curve L_P versus the deflection is not linear. But if we use only one or two compression points as done in most reported papers except for Norotte *et al.* (2008), the estimated surface tension can be more than two times smaller than the expected one. It is, for instance, the case if we use the point at deflection 30 μm corresponding to nearly a 50% deformation [see dotted line in Fig. 2(B)]. When the ELP and the CAcp (calculated on plates) are used with the angle measured on images, they give similar results to the angle independent LPF method. Values of surface tension are σ=18.5±1.5, 17.4±1, and 17.3±1 mN/m for ELP, CAcp, and LPF methods, respectively. This is in agreement with reported values for water/oil interfacial tension (du Nouy, 1925; Norotte *et al.*, 2008). Figure 2(C) shows the angle sensibility of the ELP method when the angle is not properly chosen. In this case, the surface tension varies a lot, σ=12.7±0.8, 13.0±0.8, 14.0±0.7, 16.2±0.7, and 20.8±2 mN/m for θ=0°, 10°, 20°, 30°, and 40°, respectively, while points are still linearly aligned. The error is not increasing particularly, and therefore one has to keep in mind that a low error or a linear alignment as predicted by Laplace law is not an insurance of correct surface tension measurement, using ELP method.

Embryonic F9 cell aggregates constitute the third (biological) system we investigated. Tissues display elastic behavior at short time scales (Phillips and Steinberg, 1978), which contribute to the force signal shortly after a compression step. This elasticity is usually rapidly dissipated and a force plateau is reached [see Fig. 1(E)]. We have assumed here, as it was done in previous studies (Forgacs *et al.*, 1998), that when this plateau is reached, the system is at equilibrium, which enables the surface tension measurement. We usually waited 30 min for that measurement but we also checked that even two hours after the last compression step, neither the force signal nor the aggregate shape changed within the experimental resolution.

When compressed, the aggregates show a complementary contact angle between 20° and 30° [Fig. 1(D)]. We present in Fig 2(D) the results for one aggregate (n=4 steps of compression). With such angle values, the non-angle-corrected CA method gives a much lower surface tension value (σ=3.3±0.7 mN/m) than the angle independent methods: σ=5.3±0.7 and 5.6±0.8 mN/m for LPF and CAcm, respectively [Fig. 2(D)]. When the angle measurements from the image profiles are properly taken into account, ELP and CAcp methods give similar values but with higher errors: σ=5.3±1.0 and 5.0±1.0 mN/m, respectively. Alternatively, the choice of the correct angle may be done by an adjustment of the compressions points of angle dependent and independent methods. This provides a way to evaluate the complementary angle when the image profile is not clear because it is very small (θ<10°) or because the image is partially hidden by, for instance, the upper plate, as in Fig. 1(D).

To further show the statistical difference between the results obtained with the CA methods and the LPF methods we analyzed seven different aggregates, 23 compression steps [Fig. 2(E)]. The mean surface value obtained with the CA method is 3.5±0.3 mN/m compared to 4.9±0.3 mN/m for the LPF method. The p-value obtained comparing the two results is inferior to 0.001. The seven investigated aggregates have diameters before compression in the range of 372–585 μm. Their volumes are therefore comprised between 27×10^6 and 105×10^6 μm^3 (i.e., a fourfold increase). We can conclude that the surface tension of these F9 aggregates is volume independent.

We finally confirmed our results on a different cell line: chicken embryonic neural retina cells [Fig. 2(F)]. The value of the contact angle was estimated to be around 30°. The results obtained are similar to the F9 ones. The surface tension value with the CA method is 2.1±0.3 mN/m as previously measured (Foty *et al.*, 1996), which is again lower than for the ELP end LPF method (2.7±0.3 mN/m).

In order to validate these findings, we have generated exact droplet profiles following the study of Norotte *et al.* (2008). For a given volume V, a given separation H between plates, and a given contact angle and surface tension (we used here σ=5 mN/m), the shape of the droplet and the force F exerted on the plates can be determined. We have recalculated the surface tension using the different methods by eventually introducing small errors in the input geometrical parameters (θ, see below, and H, not shown) in order to simulate the "measurement inaccuracies" of a real experiment. Of course, the ELP method gives always the exact value when we introduced the correct angle [black curves in Figs. 3(B) and 3(C)].

For a null complementary contact angle, one can appreciate in Fig. 3(A) the deviation of the real profile (green curve) to the circular arc (blue curve). The deviation is only localized in the vicinity of the plate but it results in a 15% error in the determination of R_3 used in Eq. (1) and thus in σ. This explains why the CA method based on this equation has the largest error on the surface tension even when the complementary contact angle is 0° [Fig. 3(B)]. When Eq. (2) is used, the error in σ by using the CAcm or LPF method is introduced by the measurement of R_2 itself. Both methods underestimate σ because R_2 is slightly overestimated. The deviation to the real value (σ=5 mN/m) de-

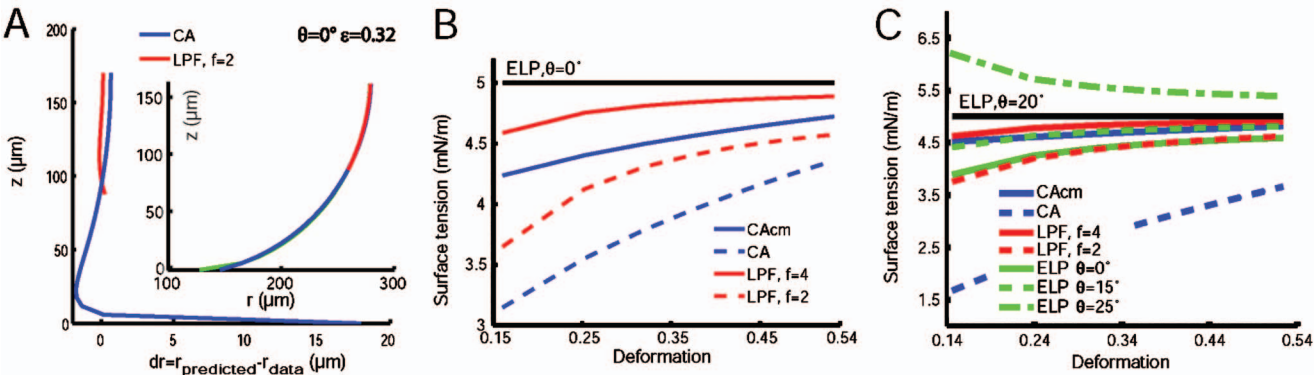

Figure 3. Tests of robustness of the different methods from a numerically generated exact droplet profile following Norotte *et al.* (2008) with a designated surface tension 5 mN/m. (A) Residual and radius (inset) of the profile estimated by the different methods for $\theta=0°$, a deformation parameter $\varepsilon=Ho-H/Ho=0.32$ (green, ELP method which gives the exact profile when contact angle is properly set; blue, CA methods showing a deviation near the plate; red, profile from a polynomial fit in a central window). Surface tension evaluation as a function of the deformation parameter (B,C) for $\theta=0°$ (B), and $\theta=20°$ (C). In the latter case we simulated compression and determined the surface tension with a deliberately incorrectly chosen θ, using the ELP method.

creases for large compressions (i.e., large deformation parameter $\varepsilon=Ho-H/Ho$, where Ho is the uncompressed aggregate height). The LPF method gives the best results when the proportion H/f of the profile around the median plane used for the local second order polynomial fit is not too large: $\sigma=4.88$ and 4.58 mN/m for $f=4$ and 2, respectively, for a large compression ($\varepsilon=0.5$). The CAcm method gives an intermediate value of 4.66 mN/m when using the full profile ($f=1$).

When the complementary contact angle is larger [i.e., $\theta=20°$, Fig. 3(C)], again the LPF method provides the best results for a narrow fitting window ($f=4$) followed by the CAcm method [Fig. 3(C)]. The error is even lower compared to the analysis where $\theta=0°$: $\sigma=4.90$ and 4.78 mN/m for the LPF ($f=4$) and CAcm methods, respectively, for $\varepsilon=0.5$. Error is much larger with the ELP method when an error of only 5° is introduced on θ: for $\theta=25°$, $\sigma=5.5$ mN/m (i.e., 10% error). The CA method using $\theta=0°$ gives completely wrong results.

DISCUSSION

In this report, we have carefully investigated the effect of the geometrical approximations on measuring the surface tension of liquids and tissues. For tissues, we have extensively studied the mouse embryonic carcinoma F9 cell line. After about 10 min compression, no net change in force [Fig. 1(E)] or in radii of curvature R_1 and R_2 was observed. In addition, the profile of these aggregates is well described by the Laplace profile [green curve in Fig. 1(D)]. The capillary laws for the compressive force [Eqs. (1) and (3), or (5) with the correct contact angle] are adjusted with a single surface tension value for different compression rates and independently of the aggregate volume [Fig. 2(D)]. Therefore the quantity we measure has all the properties of a surface tension. It may have several biological origins: cadherin expression level (Foty and Steinberg, 2005), integrin-extracellular matrix interactions (Robinson *et al.*, 2003), or cell contractility and rigidity (Harris, 1975; Brodland, 2002; Krieg *et al.*, 2008).

We have shown that when capillary laws are properly employed, the three methods to analyze surface tension from compressed droplet (ELP, LPF, and CA) give similar results with slightly different errors. Nevertheless, each method has a different sensibility to geometrical parameters, making some of them more robust than others.

To date, except in the study by Norotte *et al.* (2008), the circular arc approximation method is the only one used to measure tissue surface tension. Even when the deviation to the circular arc profile is evident near the plates [Fig. 3(A)], the radius of curvature R_2 at median plane is correctly calculated. As a result, the CAcm method, which consists in a circular arc fit combined with the force Eq. (2) at median plane, provides very acceptable results [5%–10% error on simulated drops depending on contact angle and compression rate, Figs. 3(B) and 3(C)]. The simultaneous use of Eq. (1) with $\theta=0$ and of Eq. (3) leads to some inconsistencies when the complementary contact angle actually deviates from zero. The result is that the measured surface tension is systematically lower than the actual tissue surface tension value and can lead to an underestimation of more than 100% [Figs. 2(B), 2(D), and 3(C)]. One can therefore postulate that some of the reported surface tension values are incorrect because of a finite contact angle. We want to insist on the fact that even if the errors on the surface tension appear to be as low for the CA method as for the other angle independent methods, this does not mean that the value obtained is correct as the capillary laws are not properly used.

Inserting the correct angle in Eq. (1) allows a correct estimate of σ, when using the CAcp method. However, there is no need to use Eq. (1) at the plane of the plate, because this requires the input of four geometrical parameters R_1, R_2, θ,

and H, of which especially R_2 and θ are usually measured with large errors. In contrast, the ELP method, based on the exact solution of Laplace equation, is more robust from a computational point of view. The resolution of Eqs. (4) and (5) is numerically easy and does not necessitate a least squared fit of the radius of curvature R_2 as in case of LPF or CA methods. However, we found that an error of 5° on θ introduces non-negligible relative errors on the surface tension σ (about 10%). Such an error is not particularly exaggerated for cell aggregates when θ is small because cell aggregates are rough (not as regular as fluid droplets). The contact angle may also change after several subsequent compressions. The ELP method also requires the input of the aggregate compressed height H, which may suffer errors, for instance, due to optical aberrations and hidden part of the droplets.

As a conclusion, when performing compression experiments, we strongly recommend the use of an angle independent method that requires only the two parameters R_1 and R_2. The CAcm method may have the lowest error when aggregate is symmetric but rough. Otherwise, the proposed LPF method is robust and provides the lowest error when the profile is smooth as the fitting window can be narrowed. This method is a straightforward application of Laplace equation. R_2 is measured by a second order polynomial fit at median plane. While other methods assume reflection symmetry with respect to equatorial plane, the LPF method deals naturally with up-down asymmetries in the aggregate profile. Such asymmetries may arise either because of a slightly titled field of view, non-perfectly-parallel-aligned compression plates, the effect of gravity, or because of differences in adhesion affinities and contact angles with the top and bottom compression plates. Our least-squared fit code running on Matlab is available upon request at helene.ayari@lpmcn.univ-lyon1.fr.

MATERIALS AND METHODS

The compression plate tensiometer

We designed and built our own surface tension apparatus: a droplet or aggregate is compressed between two parallel glass plates [Fig. 1(A)]. The lower compression plate consisting of a 2 mm thick borosilicate glass, is located at the bottom of a medium chamber, and is moved in the x,y,z directions through an electronic micromanipulator (MP285, Sutter Instrument). The upper compression plate, made of a cover glass, is connected through an inox wire (diameter 0.8 mm) to a copper-beryllium cantilever (spring constant $k\sim 0.36$ N/m calibrated by putting droplets of water of known volume on the cantilever). The cantilever deflection is measured with a noncontact eddy current position measurement apparatus (DT 3701-U1-A-C3, micro-epsilon). The complete setup is mounted in a thermally isolated chamber to maintain the desired temperature using a thermal resistance, which is controlled by a Lakeshore 331 apparatus. The aggregate profile is recorded using a binocular (MZ16, Leica) and a digital camera (A 686M, Pixelink). The lightning is adjusted by a KL 1500 LCD cold light source (Schott) through "flexible tubes." The whole setup is controlled with Labview and image analysis is performed with Matlab.

The chamber in which aggregates are deposited contains an opening, to facilitate displacements and choice of aggregates. The free surface is covered with a thick mineral oil layer to prevent evaporation. Glasses surfaces are carefully cleaned with soap and pure water (sonicated 30 min with 2% Microson detergent, Fisher Bioblock, France). They are first made hydrophobic by silanization with perfluorosilane (ABCR, F06179) then incubated in 10 mg/ml Pluronic F-127 (Sigma) for 5 min and finally rinsed briefly with water and dried. This treatment assures a minimum of aggregates adhesiveness. Each droplet or aggregate was subjected to at least four compressions. For tissues, we waited 30 min between two compression steps in order for the aggregate to reach force and shape equilibrium. In Fig. 1(E), we present the force signal as measured by our cantilever and position sensor: the peak of force just after a compression is followed by a force relaxation period of about 10 min.

The ELP (exact Laplace profile) method

R_1 and θ are measured directly on the images of compressed aggregates. For the determination of H, it is important to use the deflection signal to evaluate precisely the position at which the upper plate contacts the aggregate. We found that this position can be hidden on the image due to slight inclination of upper compression plate, of optical axis, or of illumination. In this study, H is determined with a resolution of about 2 μm. Following Norotte *et al.* (2008), when gravity is neglected, a dimensionless parameter α is calculated by solving numerically the following equation:

$$\frac{\mathrm{H}}{2\mathrm{R}_1}=\mathrm{f}_\theta(\alpha)=\int_{\beta(\alpha,\theta)}^{1}dx\left(\left(\frac{x}{\alpha x^2+1-\alpha}\right)^2-1\right)^{-1/2}, \quad (4)$$

where $\beta(\alpha,\theta)=(\sin(\theta)+\sqrt{\sin^2(\theta)+4\alpha(\alpha-1)})/2\alpha$ and σ is then given by

$$F=2\pi R_1(\alpha-1)\sigma=L_E\sigma. \quad (5)$$

The LPF (local polynomial fit) method

We use Eq. (2) to calculate surface tension from the measurement of the two radii of curvature R_1 and R_2 [Fig. 1(A)]. This requires the analysis of the aggregate profile $r(z)$ along vertical axis z. It is drawn by hand on the right and left sides of the aggregate. We did not make any automated contour analysis because of inhomogeneities and varying lightning conditions during subsequent compression steps.

A curve can always be approximated locally by a second order polynomial $r=az^2+bz+c$; the local radius of curvature is then given by $R_2=1/2a$. The narrower the window on which the profile will be fitted, the lower the residual

$dr = r_{predicted} - r_{data}$ on the fitted profile and the better the evaluation on the curvature will be (see Fig. 3). Of course, we are limited by the image resolution on the contour and, in the case of aggregates, by the surface roughness. This prevents us from using two small windows. In practice, this window is adjusted between one fourth and one half of the whole side contour. R_1 is then taken to be half of the distance between points having the highest r-coordinates on both right and left fitted contours.

For each side, the error of R_1 is set to the maximum value of the residual dr and the error on R_2 is given by the 95% confidence interval given on the polynomial fit using the curve fitting toolbox of Matlab. The error on both sides is averaged and divided by $2^{1/2}$. It is about 3 and 10 μm, for R_1 and R_2, respectively.

The CA (circular arc) method

The complete contour on both sides of the aggregate is approximated by a circular arc as done in previously reported studies except for Norotte *et al.* (2008). R_2 is obtained by a fit of the previously recorded profile (see LPF method section) using the function fitellipse.m under Matlab (http://www.mathworks.com/matlabcentral/fileexchange/15125). We have calculated the surface tension using this circular arc approximation in three different ways: (i) using Eq. (2), where the force is expressed at median plane (CAcm method); (ii) by combining Eqs. (1) and (3), where force is expressed on plates, with $\theta = 0°$ (original CA method); and (iii) by combining Eqs. (1) and (3) using the measured θ (CAcp). R_1 is obtained in the same way for ELP, LPF, and CA methods. When it is needed, i.e., for the CA and CAcp methods, H is obtained as explained in the ELP method section.

Statistical analysis

The value of σ is calculated from the linear fit from the curve L_P, L_M, or L_E defined in Eqs. (1) and (3), or (5) as a function of the deflection (see Fig. 2). Indeed, the slope corresponds to k/σ. Errors $\Delta\sigma$ are calculated from the 95% confidence interval on fitted slopes by the curve fitting toolbox of Matlab (relative errors on slopes are the same as relative error on sigma as the relative error on k is negligible).

The comparison between surface tension values obtained with CA methods and the one obtained with angle independent methods was done with a Kruskal-Wallis nonparametric test. As the Kruskal-Wallis test was found significant ($P < 0.05$), a Wilcoxon nonparametric test was performed (R 2.6.0, R foundation for statistical computing, Vienna, Austria). P values < 0.001 were considered as significant and noted with three stars.

Aggregate formation statistical analysis

Mouse embryonic carcinoma F9 cell line was a generous gift from S. Nagafuchi (Nagafuchi *et al.*, 1987). Cells were maintained in DMEM (41965-039, GIBCO) supplemented with 10% foetal bovine serum (2902 P-241021, Biotech GmbH). For the aggregate formation, cells were dissociated and reassemble in 25 μl hanging drops containing between 1,000 and 8,000 cells (Robinson *et al.*, 2003). After 2 days, the newly formed aggregates were transferred to 24 well plates containing fresh medium and then put on a gyratory shaker for 2 more days. For the compression measurements, the cell aggregates were transferred to CO_2 independent medium (18045-054, GIBCO).

Chicken embryonic neural retina cell's aggregate were prepared as described in Mombach *et al.* (2005). Aggregates were cultured in BME (41010, Gibco) with 10% FCS (3302—P281501, biotech GmbH).

ACKNOWLEDGMENTS

This project was funded by the ANR "Jeunes chercheuses Jeunes Chercheurs" 2005. The research team belongs to the CNRS consortium CellTiss. A.M., H.D.-A., and J.-P.R.. designed the study; A.M. performed the experiments and the analysis. H. D.-A. contributed to data analysis and J.-P.R. wrote the manuscript. We would like to thank Professor A. Nagafuchi (Kumamoto University, Japan) for a generous gift of F9 cell line. We thank J. Käfer, L. Bocquet, E. Charlaix, and T. Biben for useful discussions and G. Forgacs, F. Graner, and G. Krens for their useful comments on the manuscript. Competing interests statement: The authors declare no competing interests.

REFERENCES

Beysens, DA, Forgacs, G, and Glazier, JA (2000). "Cell sorting is analogous to phase ordering in fluids." *Proc. Natl. Acad. Sci. U.S.A.* **97**, 9467–9471.

Brodland, GW (2002). "The differential interfacial tension hypothesis (DITH): a comprehensive theory for the self-rearrangement of embryonic cells and tissues." *J. Biomech. Eng.* **124**, 188–197.

Brodland, GW, Chen, DI, and Veldhuis, JH (2006). "A cell-based constitutive model for embryonic epithelia and other planar aggregates of biological cells." *Int. J. Plast.* **22**, 965–995.

Cui, C, Yang, X, Chuai, M, Glazier, JA, and Weijer, CJ (2005). "Analysis of tissue flow patterns during primitive streak formation in the chick embryo." *Dev. Biol.* **284**, 37–47.

Davis, GS, Phillips, HM, and Steinberg, MS (1997). "Germ-layer surface tensions and 'tissue affinities' in *Rana pipiens* gastrulae: quantitative measurements." *Dev. Biol.* **192**, 630–644.

du Nouy, PL (1925). "An interfacial tensiometer for universal use." *J. Gen. Physiol.* **7**, 625–632.

Forgacs, G, Foty, RA, Shafrir, Y, and Steinberg, MS (1998). "Viscoelastic properties of living embryonic tissues: a quantitative study." *Biophys. J.* **74**, 2227–2234.

Foty, RA, Forgacs, G, Pfleger, CM, and Steinberg, MS (1994). "Liquid properties of embryonic tissues: measurement of interfacial tensions." *Phys. Rev. Lett.* **72**(14), 2298–2301.

Foty, RA, Pfleger, CM, Forgacs, G, and Steinberg, MS (1996). "Surface tensions of embryonic tissues predict their mutual envelopment behavior." *Development* **122**, 1611–1996.

Foty, RA, and Steinberg, MS (2004). "Cadherin-mediated cell-cell adhesion and tissue segregation in relation to malignancy." *Int. J. Dev. Biol.* **48**, 397–409.

Foty, RA, and Steinberg, MS (2005). "The differential adhesion hypothesis: a direct evaluation." *Dev. Biol.* **278**, 255–263.

Gordon, R, Goel, NS, Steinberg, MS, and Wiseman, LL (1972). "A rheological mechanism sufficient to explain the kinetics of cell sorting." *J. Theor. Biol.* **37**, 43–73.

Harris, A (1975). "Is cell sorting caused by differences in the work of intercellular adhesion? A critique of the Steinberg hypothesis." *J. Theor. Biol.* **61**, 267–285.
Hegedüs, B, Marga, F, Jakab, K, Sharpe-Timms, KL, and Forgacs, G (2006). "The interplay of cell-cell and cell-matrix interactions in the invasive properties of brain tumors." *Biophys. J.* **91**, 2708–2716.
Jakab, K, Damon, B, Marga, F, Doaga, O, Mironov, V, Kosztin, I, Markwald, R, and Forgacs, G (2008a). "Relating cell and tissue mechanics: implications and applications." *Dev. Dyn.*, **237**, 2438–2449.
Jakab, K, Norotte, C, Damon, B, Marga, F, Neagu, A, Besch-Williford, CL, Kachurin, A, Church, KH, Park, H, Mironov, V, Markwald, RR, Vunjak-Novakovic, G, and Forgacs, G (2008b). "Tissue engineering by self-assembly of cells printed into topologically defined structures." *Tissue Eng.*, **14**, 413–421.
Jakab, K, Neagu, A, Mironov, V, Markwald, RR, and Forgacs, G (2004). "Engineering biological structures of prescribed shape using self-assembling multicellular systems." *Proc. Natl. Acad. Sci. U.S.A.*, **101**, 2864–2869.
Kalantarian, A, Ninomiya, H, Saad, SM, David, R, Winklbauer, R, and Neumann, AW (2009). "Axisymmetric drop shape analysis for estimating the surface tension of cell aggregates by centrifugation." *Biophys. J.*, **96**, 1606–1616.
Krieg, M, Arboleda-Estudillo, Y, Puech, PH, Käfer, J, Graner, F, Müller, DJ, and Heisenberg, CP (2008) "Tensile forces govern, germ-layer organization in zebrafish." *Nat. Cell Biol.* **10**, 429–436.
Lecuit, T, and Lenne, PF (2007). "Cell surface mechanics and the control of cell shape, tissue patterns and morphogenesis." *Nat. Rev. Mol. Cell Biol.* **8**, 633–644.
Marga, F, Neagu, A, Kosztin, I, and Forgacs, G (2007). "Developmental biology and tissue engineering." *Birth Defects Res. C* **81**, 320–328.
Mombach, JCM, Robert, D., Graner, F, Gillet, G, Thomas, GL, Idiart, M, and Rieu, JP (2005). "Rounding of aggregates of biological cells: Experiments and simulations." *Physica A* **352**, 525–534.
Nagafuchi, A, Shirayoshi, Y, Okazaki, K, Yasuda, K, and Takeichi, M (1987). "Transformation of cell adhesion properties by exogenously introduced E-cadherin cDNA." *Nature (London)* **329**, 341–343.
Norotte, C, Marga, F, Neagu, A, Kosztin, I, and Forgacs, G (2008). "Experimental evaluation of apparent tissue surface tension based on the exact solution of the Laplace equation." *EPL* **81**, 46003.
Phillips, HM, and Steinberg, MS (1978). "Embryonic tissues as elasticoviscous liquids. I: Rapid and slow shape changes in centrifuged cell aggregates." *J. Cell. Sci.* **30**, 1–20.
Rieu, JP, and Sawada, Y (2002). "Hydrodynamics and cell motion during the rounding of 2D hydra cell aggregates." *Eur. Phys. J. B* **27**, 167–172.
Robinson, EE, Zazzali, KM, Corbett, SA, and Foty, RA (2003). "$\alpha 5\beta 1$ integrin mediates strong tissue cohesion." *J. Cell. Sci.* **116**, 377–386
Ryan, PL, Foty, RA, Kohn, J, and Steinberg, MS, (2001). "Tissue spreading on implantable substrates is a competitive outcome of cell-cell vs. cell-substratum adhesivity." *Proc. Natl. Acad. Sci. U.S.A.* **98**, 4323–4327.
Schötz, E, Burdine, RD, Jülicher, F, Steinberg, MS, Heisenberg, CP, and Foty, RA (2008). "Quantitative differences in tissue surface tension influence zebrafish germ layer positioning." *HFSP J.* **2**, 42–56.
Steinberg, MS (1962). "On the mechanism of tissue reconstruction by dissociated cells. III: Free energy relations and the reorganization of fused, heteronomic tissue fragments." *Proc. Natl. Acad. Sci. U.S.A.* **48**, 1769–1776.
Steinberg, MS (1963). "Reconstruction of tissues by dissociated cells: some morphogenetic tissue movements and the sorting out of embryonic cells may have a common explanation." *Science* **141**, 401–408.
Steinberg, MS (1970). "Does differential adhesion govern self-assembly processes in histogenesis? Equilibrium configurations and the emergence of a hierarchy among populations of embryonic cells." *J. Exp. Zool.* **173**, 395–434.
Technau, U, and Holstein, TW (1992). "Cell sorting during the regeneration of hydra from reaggregated cells." *Dev. Biol.* **151**, 117–127.
Winters, BS, Shepard, SR, and Foty, RA (2005). "Biophysical measurement of brain tumor cohesion." *Int. J. Cancer* **114**, 371–379.